3D distribution models of Ca, Cr, and Fe in a magnetic CP star atmosphere with anisotropic wind

G. Alecian, M. J. Stift

Monthly Notices of the ROYAL ASTRONOMICAL SOCIETY

MNRAS **504,** 1370–1378 (2021) doi:10.1093/mnras/stab952
Advance Access publication 2021 April 8

3D distribution models of Ca, Cr, and Fe in a magnetic CP star atmosphere with anisotropic wind

G. Alecian [1]★ and M. J. Stift[2]

[1] *LUTH, Observatoire de Paris, PSL Research University, CNRS, Université Paris Diderot, 5 place Jules Janssen, F-92190 Meudon, France*
[2] *Kuffner-Sternwarte, Johann Staud-Strasse 10, A-1160 Wien, Austria*

Accepted 2021 March 29. Received 2021 March 22; in original form 2021 March 4

ABSTRACT

We present time-dependent atomic diffusion calculations for Ca, Cr, and Fe in a stellar magnetic atmosphere including an anisotropic wind. For three different models of mass-loss rates (or wind), we obtain a 3D description of the entire atmosphere. In two of these models, the mass-loss rate varies according to the magnetic field inclination, the assumed field geometry being non-axisymmetric. When the dipolar component of the magnetic field dominates, we find that ring-like abundance structures will be prominent. Spot-like distributions can also exist according to the field geometry. Abundance distributions turn out to be highly sensitive to the mass-loss model. The results are discussed and compared to an observational model of a real chemically peculiar star (θ Aurigae) that features parameters close to those of the model we have adopted for our calculations.

Key words: diffusion – magnetic fields – stars: abundances – stars: chemically peculiar – stars: mass-loss.

1 INTRODUCTION

Among main-sequence stars, only magnetic chemically peculiar stars (ApBp stars) are clearly known to exhibit inhomogeneous distributions of elements over their surface. The magnetic peculiarities and the unusual spectral features of ApBp stars have been studied since the late 1940's mainly by Babcock (1947), Stibbs (1950), Deutsch (1956), Deutsch (1957). These pioneering works have led to the development of the framework of the magnetic oblique rotator model for ApBp stars, followed all along later years by numerous publications with impressive improvements of observational and modelling techniques. On the theoretical side, work calling on atomic diffusion and devoted to chemically peculiar (CP) stars started with Michaud (1970), and for magnetic atmospheres with Vauclair, Hardorp & Peterson (1979), Michaud, Charland & Megessier (1981), and Alecian & Vauclair (1981). More than four decades later, the theoretical basis of atomic diffusion processes remains more or less unchanged. However, numerical models have made huge progress since, as has happened in most other scientific fields. First, 3D numerical models for the distribution of metals in a non axi-symmetric magnetic atmosphere appeared a few years ago (Alecian & Stift 2017). In these calculations, the 3D abundance distributions (equilibrium solutions) were obtained by reconstruction from a relatively large grid of 1D LTE models. Soon after, the effect of mass-loss was included in time-dependent 1D calculations of atomic diffusion in magnetic atmospheres by Alecian & Stift (2019). In that latter paper, it was shown that some of the observed superficial abundances can only be explained by invoking the occurrence of mass-loss in addition to atomic diffusion. In this work, we continue on this path, considering for the first time 3D time-dependent models including mass-loss.

Among the most recent observational results, let us quote Kochukhov, Shultz & Neiner (2019), who studied two magnetic Ap stars (θ Aurigae and ϵ Ursae Majoris), proposing maps of their magnetic field and maps of the respective abundance distributions of Cr and Fe. Here it is necessary to remind the reader that Michaud, Alecian & Richer (2015) have stressed the impossibility to derive detailed theoretical models for individual stars with present-day means, since the evolution of abundance distributions due to atomic diffusion is extremely sensitive to any physical process missing in the modelling procedure, including mixing motions that are generally not easy to predict and not measured in observations. Therefore, the purpose of this paper is to carry out calculations for stars that only look like θ Aurigae, but not precisely for this star. We present a theoretical model of Ca, Cr, Fe distributions in atmospheres permeated by a non-axisymmetric magnetic field of moderate intensity, using the most advanced numerical code we have developed for magnetic stellar atmospheres, featuring time-dependent atomic diffusion together with mass-loss. In Section 2, we present some theoretical and numerical aspects of our code; in Section 3, we describe the parameters adopted for the atmosphere. Results of the computations are shown in Section 4 and discussed in Section 5.

2 THE 3D CHALLENGE

The basic approach in computing atomic diffusion in stellar atmospheres (we will not describe it here in detail) consists in first calculating radiative accelerations of atoms for the species considered, and thence their diffusion velocities (Alecian & Stift 2004, 2006). In a second step, one has to estimate the resulting abundance stratification.

★ E-mail: georges.alecian@obspm.fr

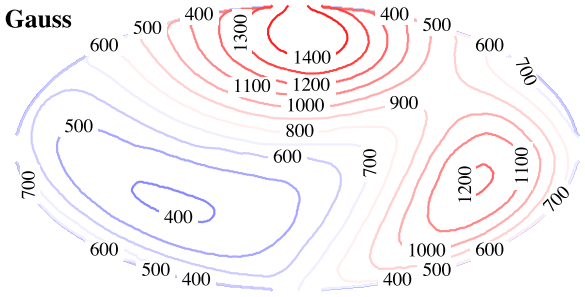

Figure 1. Contour map (Hammer equal-area projection) of the magnetic field strength used for our modelling. The field strength map is based on the magnetic model for HD 154708 (Stift et al. 2013), multiplied by a constant factor of 0.451.

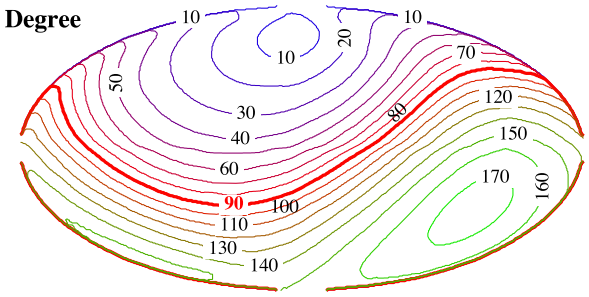

Figure 2. Same as Fig. 1 but for the angle of the magnetic field (non-axisymmetric geometry) with respect to the surface vertical. The 'magnetic equator' is given by the heavy red contour line (90°).

This can be carried out by assuming equilibrium solutions[1] (see for instance LeBlanc et al. 2009; Alecian & Stift 2010) or time-dependent calculations[2] (Alecian, Stift & Dorfi 2011; Alecian & Stift 2017). This latter approach is certainly, despite numerical difficulties, the best since particle number conservation is taken into account all along the temporal evolution of abundances.

For an axisymmetric centred dipole field, it is sufficient to carry out 2D (depth versus distance to the magnetic pole) calculations, establishing abundance stratification along the magnetic meridian. Alecian & Stift (2010) have first shown such results for a number of different effective temperatures. Numerical calculations for non-axisymmetric dipole geometries require a more sustained effort since they can address only a particular field geometry. Alecian & Stift (2017) have computed the 3D distribution of Cr and Fe for just one atmospheric model, assuming equilibrium solutions to the vertical abundance stratifications. To obtain a 3D description of the chemical structure of the atmosphere, they assumed that the whole stellar surface may be considered as a juxtaposition of independent facets[3] (with the thickness of the stellar atmosphere model), each of them calculated under the approximation of a plane-parallel atmosphere (as done by Alecian & Stift 2010). A smooth continuous abundance distribution is obtained by geometrical interpolation between facets for all layers (each layer being defined according to its optical depth at 5000 Å). In this work, we have followed a similar approach, but the structure of the individual facets results from 1D time-dependent diffusion (as done by Alecian & Stift 2019). Again, the 3D distribution of abundances is obtained by interpolation for each facet in the grid of models.

Concerning the grid of 1D models mentioned above, they were computed with our CARATMOTION code (Alecian & Stift 2019); two parameters are varied: the modulus of the magnetic field vector and its angle with respect to the vertical.[4] In Alecian & Stift (2017), the grid was composed of 81 models without mass-loss (10 field intensities with 8 angles, plus 1 model for the zero field case). In this work, a third parameter has to be added: the mass-loss rate that depends on the magnetic field vector inclination (see Section 3.2). Due to the fact that computing such a grid is numerically very expensive, we have for this study carefully adapted the grid size to the star considered (see Section 3).

3 MAGNETIC GEOMETRY AND MASS-LOSS

3.1 The adopted magnetic geometry and model of atmosphere

For this work, we have kept to the magnetic field geometry adopted by Alecian & Stift (2017). This field geometry that has been proposed for HD 154708 by Stift et al. (2013), represents a tilted, decentred dipole. It is non-axisymmetric and probably not untypical for ApBp stars. It is unfortunate that we had to refrain from considering other published geometries, since these are to be found exclusively in the form of graphical maps of abundances and of magnetic field components. It is a pity that almost the totality of these is unavailable in numerical form; not even the coefficients of the spherical harmonics fit to the magnetic fields can be found in any publicly accessible data base apart from Oksala et al. (2018). This is a serious problem, that makes it virtually impossible to independently verify Zeeman Doppler results, but it also hampers advances in the modelling of observable spectral signatures of magnetic CP stars. Wanting to compare our results to some observed star, we have scaled the magnetic field intensity of HD 154708 by a factor of 0.415, leading to a maximum field strength at the strong magnetic pole of 1.5 kG (see Figs 1 and 2). In addition, we have chosen the following stellar parameters: $T_{\rm eff} = 10\,500$ K, $\log g = 3.6$. Note that the atmospheric model thus adopted is not far removed from the one for θ Aurigae discussed by Kochukhov et al. (2019). Our code CARATMOTION recomputes the atmosphere at each time-step with Kurucz's ATLAS12 code (Bischof 2005; Kurucz 2005), maintaining effective temperature and gravity, but taking into account the change in the abundance distributions of Ca, Cr, Fe (for the other elements we assume no temporal change in the solar abundances proposed by Asplund et al. 2009). The underlying hypothesis is that the abundance changes in the atmosphere do not affect the global stellar structure, and that this structure does not significantly evolve during the age interval of

[1]Equilibrium solutions correspond to local abundances calculated such that radiative acceleration vector is everywhere exactly opposite to gravity (approximately equivalent to zero diffusion velocity). Another option would consist in imposing zero diffusion velocity, which leads to the radiative acceleration vector directed approximately opposite to gravity. Both options are equivalent, provided that thermal diffusion, the effect of a concentration gradient, and other microscopic processes (ambipolar diffusion, light induced drift, etc.) are negligible.

[2]Time-dependent solutions are obtained by solving the continuity equation. Ideally that leads to stationary solutions with constant atomic flux throughout the stellar atmosphere.

[3]These facets can be assumed to be independent from each other because the horizontal diffusion time-scale is much larger than the vertical one that we consider.

[4]For a symmetric dipole, an angle of 0° corresponds to a magnetic pole, 90° to the magnetic equator.

the calculation. This is consistent with keeping abundances solar at the bottom boundary. Note also that diffusion models for ApBp stars assume that no mixing occurs in their atmospheres. Apart from theoretical arguments developed following Michaud (1970), confirmation for this has come from the detection of clear signs of abundance stratifications in observed spectra (see, e.g. Ryabchikova 2005 or Ndiaye, LeBlanc & Khalack 2018), abundance stratifications excluding mixing. Therefore, neither rotation nor convection are considered in our atmospheric model.

3.2 Models with mass-loss

Ever since the 1970s, it has been proposed to consider mass-loss together with atomic diffusion (see Vauclair 1975; Michaud et al. 1983; Babel 1992; Alecian 1996; Landstreet, Dolez & Vauclair 1998; Vick et al. 2010; Alecian 2015). In the present context, mass-loss must be understood as a flux of matter, all atomic species moving at the same velocity. This general flux is assumed constant with depth and time, without any further considerations concerning the details of the physics of its origin, or the way the momentum is homogeneously distributed among the species. The velocity of particles due to mass-loss corresponds to the velocity of a wind that has to be added to the specific diffusion velocities; it is only determined by the mass-loss rate and the local mass density.

There are no direct observations of stellar winds available for these stars. This can be explained quite naturally, since the mass-loss rates considered are too weak to be detected. The various theoretical models we mentioned above have shown that the mass-loss rates should be around 10^{-13} solar mass per year, or much smaller, in order to remain compatible with diffusion processes. Larger mass-loss prevents the build-up of abundance stratifications.

Only quite recently has mass-loss been introduced into time-dependent calculations for atmospheres. Alecian & Stift (2019) have shown quantitatively that some of the abundances observed in CP stars cannot be explained without taking into account the competition between atomic diffusion and mass-loss. Indeed, in non-magnetic CP stars (HgMn stars), the slight underabundance often observed for magnesium is well explained in their simulations for a star with parameters close to $T_{\rm eff} = 12\,000$ K and $\log g = 4.0$, if a mass-loss rate of $0.425\,10^{-13}$ solar mass per year is imposed; larger values let magnesium keep its solar abundance, whereas lower values cause important depletions that have never been observed. On the other hand, Babel (1992), in his study of 53 Cam, proposed that mass-loss has to be anisotropic in magnetic stars, with a higher rate near the magnetic pole than around the magnetic equator. In his model, he divided the star into two zones (see his fig. 6), one cap-like around the magnetic poles, the other belt-like including the equator. In his model, mass-loss occurs only in the polar caps.

We have carried out our calculations for three models of mass-loss shown in Fig. 3. Models A and B follow the same approach as Babel (1992): The mass-loss rate (in solar mass per year) is maximum at the magnetic pole ($1.\,10^{-13}$) and decreases slowly until the field angle reaches 30°; it decreases faster until 85° where its reaches its minimum value ($0.1\,10^{-13}$ for model A, $0.3\,10^{-13}$ for model B). Unlike Babel (1992), the minimum mass-loss rate we impose is not zero because our numerical simulations often can become unstable when the mass-loss rate is too low, generally at high inclination angles (close to the magnetic equator), but occasionally also at other angles. This is also why model C – for which we would have preferred to impose zero mass-loss – features a non-zero constant mass-loss of $0.2\,10^{-13}$ (corresponding to the minimum value that ensures acceptable convergence over most of the surface area, at least for Cr).

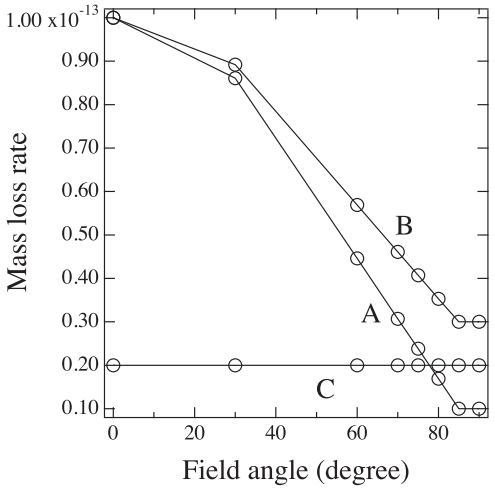

Figure 3. Three models (A, B, and C) of mass-loss rates (in solar mass per year) as a function of magnetic field angle with respect to the vertical. Open circles point out the positions of 1D models inside the grid; each of these has also been calculated for 10 values of the magnetic field intensity (see the text).

4 RESULTS

4.1 Numerical calculations

Our results for the three models of mass-loss shown in Fig. 3 are displayed in Figs 4–7 for Ca, Cr, and Fe respectively. As in Alecian & Stift (2017), the 3D element distributions are presented in a tomographic view where the atmosphere is divided into six slabs according to the optical depth $\log \tau_{5000}$. The abundance attributed to each slab is the averaged abundance over the layers inside of each slab. We want to recall that in Alecian & Stift (2017) Cr and Fe distributions are equilibrium solutions in a static atmosphere, whereas in this work, results have been obtained with the help of time-dependent diffusion calculations, mass-loss included. We also have to point out that even if the magnetic geometry is identical in both works, the field intensity has been scaled with different factors. Therefore, the respective distributions of Cr or Fe must not be compared.

The distributions shown in Figs 4–7 have been obtained considering the simultaneous diffusion of Ca, Cr and Fe. At the first time-step ($t = 0.0$), abundances are supposed homogeneous and solar throughout the atmosphere. The final time-steps roughly correspond to $t \approx 10^5$ yrs depending on the model inside the grid of 1D models (see Section 2). Actually, our calculations have been stopped either when diffusion fluxes became stationary, or because the CPU time limit had been reached. This fluctuates from model to model inside the grid. For a result to be considered satisfactory, we require that a stationary solution be reached (±10 per cent constant particle flux) for $\log \tau_{5000} < 1.0$. Stationary solutions would be hard to obtain deeper down in the atmosphere: diffusion time-scales become very large in the deepest layers of the atmosphere, and our boundary condition at the bottom assumes a constant solar abundance (see the discussion of boundary conditions in section 3.1 of Alecian et al. 2011). In some 1D models of the grid, for some of the considered elements, the calculations did not reach a stationary solution. This

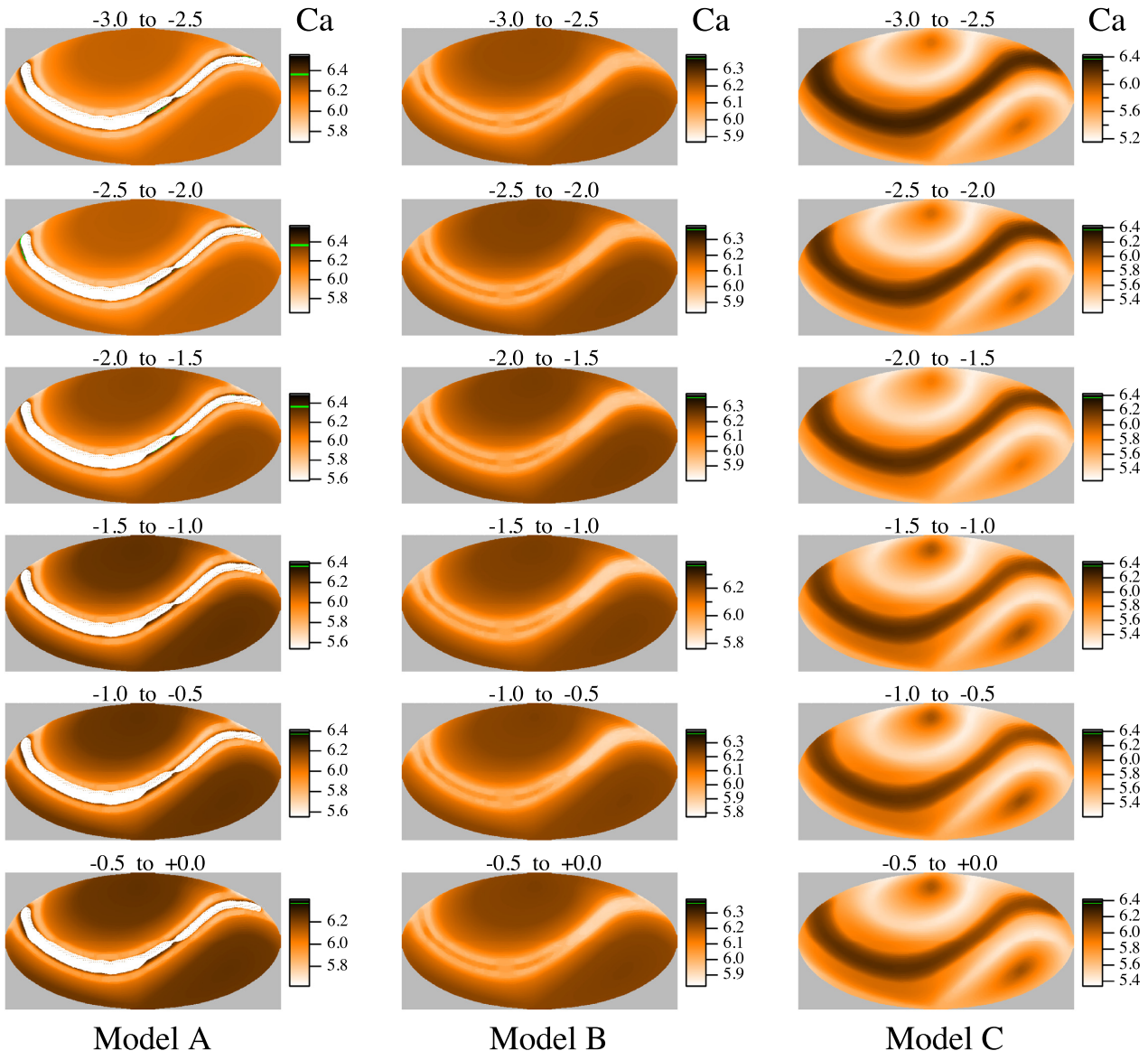

Figure 4. Tomographic view of the Ca abundance (Hammer equal-area projection) for mass-loss models A, B, and C. Six slabs (actually spherical shells) corresponding to six contiguous optical depth ranges (indicated above each panel) per model are shown in each column. Note that the relation between abundances and colour scale differs from one panel to the other. The solar abundance (log number of atoms relative to H) of Ca is 6.36 (on the usual scale with H = 12). The green colour in the colour wedges marks positions where the Ca abundance is solar ±5 per cent; this colour however never appears in our panels since Ca is underabundant everywhere. The blank (white) zones for equatorial regions of model A correspond to those for which our numerical simulations have not reached a stationary solution (see text).

usually occurs when abundance gradients that form during the stratification build-up become too strong in optically thin layers. In that case, the algorithm implemented in CARATMOTION drastically reduces the time-step to prevent numerical instability, resulting in a virtual standstill of the temporal evolution of the model. Generally, such events are a possible herald of a physical instability as discussed in Alecian et al. (2011). The regions of the atmosphere concerned by a lack of stationarity are kept blank in our figures. Note that numerical simulations converge well for Cr for all three mass-loss models, because the stationary solution for Cr is reached prior to a possible stop of the code due to the decrease of the time-step triggered by Ca or Fe. Convergence for all three elements together has been obtained only for mass-loss model B.

4.2 Element distributions

4.2.1 Calcium

The stationary abundance of calcium we obtained is lower than its solar abundance (6.36 in units of H = 12, marked in green) over almost the whole atmosphere and for the three mass-loss models, except in very small regions hardly noticeable in Fig. 4. At first glance, this is not surprising, since Ca is only weakly supported by radiative forces; in an atmosphere with our adopted parameters, the dominating ionisation stage is Ca III (with Ar-like noble gas configuration). However, the situation is more complex because the process is strongly non-linear (see discussion in Alecian et al. 2011): actually, the radiative acceleration exceeds gravity for

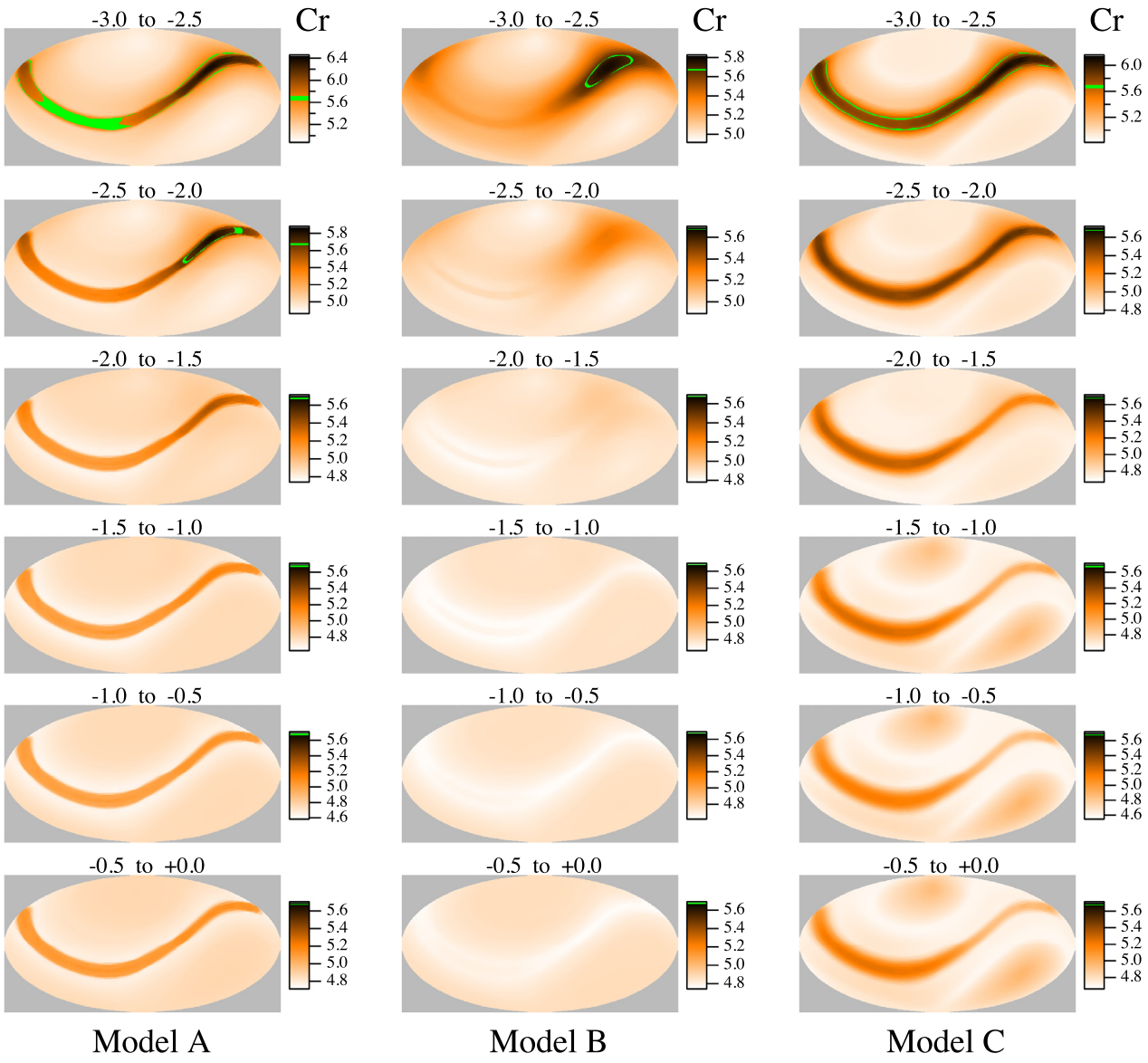

Figure 5. Same as Fig. 4, for Cr. The green colour marks positions where the Cr abundance is solar (5.67 ± 5 per cent). Note that Cr is underabundant in all slabs with $\log \tau \gtrsim -2.0$.

$\log \tau_{5000} \lesssim -2.0$. This is due to the increasing contribution of Ca II whose acceleration ensures that Ca is supported by the radiation field in these high-lying layers. We recall that our calculations are carried out in LTE approximation, and that radiative accelerations of calcium in upper layers may be significantly affected by NLTE effects (Borsenberger, Praderie & Michaud 1981). From here, we can consider that Ca escapes into the interstellar medium even at the magnetic equator, helped by the wind resulting from mass-loss. Weak radiative acceleration dominates in deeper layers ($\log \tau_{5000} > -2.0$) due to Ca III as first mentioned, and so calcium depletion cannot be compensated by diffusion from below. This leads to a general depletion of Ca. One cannot exclude a mild overabundance of Ca for model A in the equatorial region; calculations of 1D models inside our grid however did not converge for the corresponding local parameters. In model B, the underabundance of Ca is more noticeable than in the polar caps (in contrast to model C).

4.2.2 Chromium

Chromium also appears most often depleted in our stationary solutions (Fig. 5). In contrast to Ca, Cr is well supported by the radiation field (the modulus of the radiative acceleration vector is larger than gravity). Therefore, the chromium diffusion flux is always positive; the element escapes from the atmosphere except for models A and B in a small equatorial region with a moderate magnetic intensity of ≈500 G and $\log \tau_{5000} \lesssim -2.5$. In that region, the incoming flux from deeper layers of Cr enriched material cannot be counterbalanced by the escaping flux. This overabundant region (horizontal transition zone with solar abundance appears in green) might possibly be observed as a patch of Cr. In model B, the lowest abundances are found in equatorial regions with $\log \tau_{5000} > -2.0$, whereas they are highest for models A and C.

To better understand how Cr stratifies, we show in Fig. 6 two probes in-depth through the atmosphere presented in Fig. 5 (model B

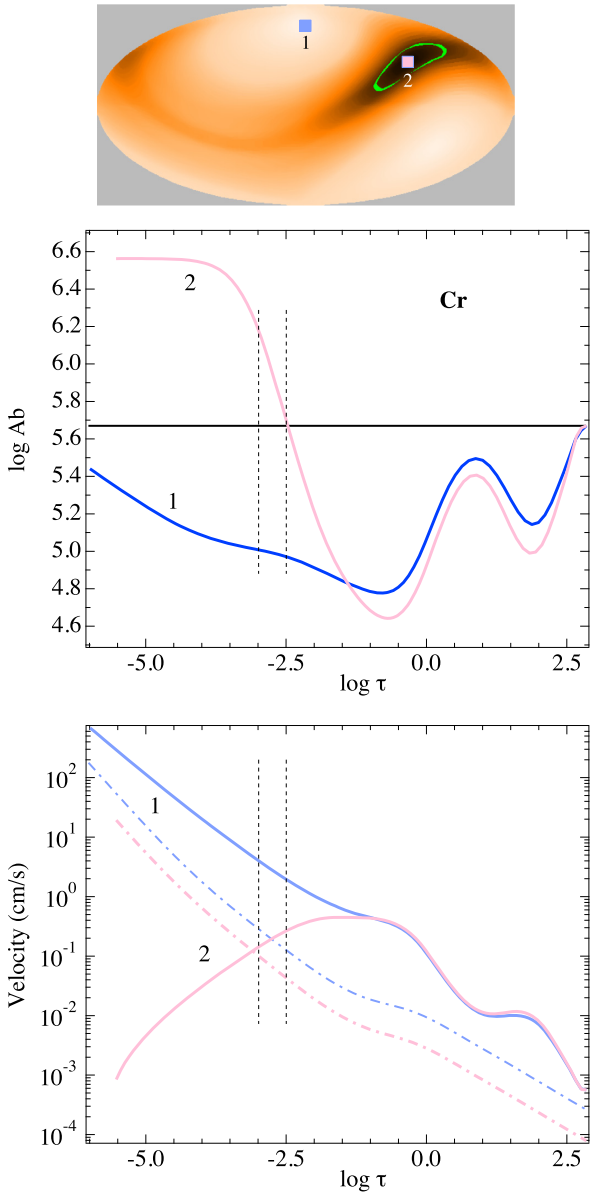

Figure 6. Chromium stratification along two stellar radii in our atmospheric model. The top panel shows the positions (points 1 and 2) for probing the atmosphere (see the text). The middle panel presents the chromium abundance stratifications at the last time-step, with the blue line corresponding to point 1, and the pink line to point 2. The horizontal solid black line represents the initial solar abundance. The vertical dashed lines show the limits of the slab of the top panel. The bottom panel displays the diffusion velocities. The point-dashed lines are the anisotropic wind velocities (model B).

using a tomographic view). The top panel is the same panel as in Fig. 5 (slab −3.0 to −2.5) with two small coloured squares identifying two points on the stellar surface: a light blue one labelled 1, and a pink one labelled 2. The magnetic parameters of point 1 are 1500 G, 0° (a magnetic pole), with a mass-loss rate of 10^{-13} solar mass per year. For point 2, we have 925 G, 90°, and $3.0\,10^{-14}$, respectively. The middle panel presents the final abundance stratification of Cr (after some 10^5 yr of diffusion) along the stellar radius passing through the centre of the small squares (curves labelled 1 and 2). The limits of the slab corresponding to the top panel is indicated by the two dashed lines (notice that abundances shown in the top panel represent the average abundances between these two dashed lines). For the sake of simplicity, we do not show the other slab limits that can be easily guessed in the plot. The bottom panel shows in the same way the diffusion velocity, plus the wind velocity corresponding to the mass-loss rates of model B.[5] The drastic drop of the diffusion velocity (curve 2) above $\log \tau_{5000} \approx -2.0$ is due to the effect of horizontal magnetic lines on the diffusion coefficient. This drop would occur higher up in the atmosphere for lower magnetic field strength, except for field lines with 0° inclination for which the diffusion coefficient does not feel the magnetic field.[6] The building up of the chromium cloud, visible in the top panel, is clearly due to the strong ascending flux of Cr atoms in layers around $\log \tau_{5000} \approx -2.0$ and the decrease of the outgoing flux above $\log \tau_{5000} \approx -3.0$. Since the diffusion velocity is still larger than the wind velocity at the bottom of the slab and decreases rapidly, the outgoing flux due to mass-loss is weaker than the incoming diffusion driven flux, which produces a local accumulation of Cr.

4.2.3 *Iron*

Iron appears to be overabundant (Fig. 7) above $\log \tau_{5000} \approx -1.0$ for the three mass-loss models (note that the green colour is always at the bottom of the colour wedges). For model B, we find an overabundant ring (of up to about +0.5 dex) on the magnetic equator for upper layers, while the same ring is found more depleted for $\log \tau_{5000} > -1.0$ than in other regions. Calculations did not converge sufficiently for models A and especially C (large blank patches in the plots). Some spot-like enhancement of iron abundance can however be guessed for the latter in some parts of the magnetic equator.

5 DISCUSSION

5.1 General behaviour

In all cases computed here, we find that the magnetic geometry has a strong impact on abundance distributions. Indeed, the maps always clearly show places where the magnetic field inclination is close to 90°, either by overabundance or by underabundance. Therefore, ring-like structures are prominent. This is not surprising since it is known that the diffusion velocity of charged particles is strongly impeded – especially in high-lying layers – when the velocity vector is more or less perpendicular to the magnetic field lines (Vauclair et al. 1979; Alecian & Vauclair 1981; Michaud et al. 1981). Such a ring-like structure should thus turn up whenever the dipolar component of stellar magnetic field is strong enough, which is the case in general. It has however to be pointed out that abundances are not homogeneous inside the ring-like structures because the field intensity is not uniform along regions where the field vector is horizontal. For instance, the Cr distribution for $\log \tau_{5000} < -2.0$ is much less depleted (and even enhanced) in some portions of the ring-like structure for model B; here the abundance inhomogeneity looks like a spot.

Besides the ring-like structures mentioned above, one also finds cap-like regions around the magnetic poles. They are essentially due to the Zeeman splitting of atomic transitions, which amplifies radiative accelerations (Alecian & Stift 2004) ever more efficiently as one approaches the magnetic poles (higher field intensity).

[5]We recall that the wind velocity is obtained by dividing the mass-loss rate by the local mass density; see equation (1) of Alecian & Stift (2019). The flux of mass-loss is assumed constant with respect to depth.
[6]The drop is less and less drastic, as the inclination decreases from 90° to 0°.

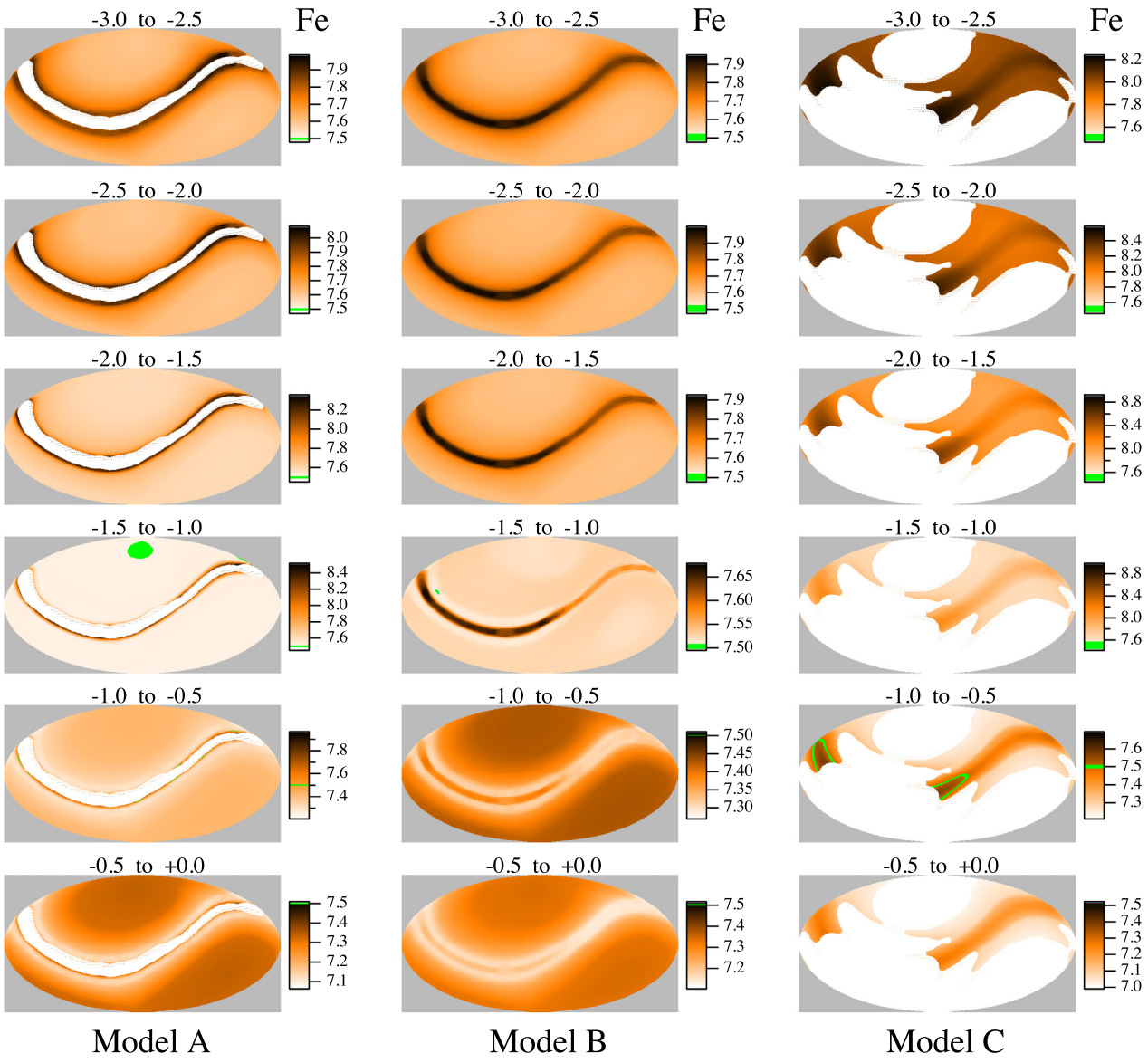

Figure 7. Same as Fig. 4, for Fe. The blank (white) zones for models A and C correspond to regions for which our numerical simulations have not reached stationary solutions (see the text). The solar abundance 7.5 (in green) is only preserved in one polar region (A, −1.5 to 1.0) and very partially in two equatorial regions (B, −1.5 to 1.0; C, −1.0 to −0.5).

Another striking aspect of our results is the importance of mass-loss and the sensitivity to its anisotropy when we compare abundance distributions obtained for the three models. This confirms the suggestion of Babel (1992), who found that in order to explain the abundances of 53 Cam, one needs to assume an anisotropic wind together with atomic diffusion. Babel considered a lower mass-loss rate compared to ours, but keep in mind that 53 Cam features a cooler atmosphere than our model and that Babel's abundances are equilibrium solutions.

5.2 Comparison with θ Aurigae

The aim of our efforts in numerical modelling of atomic diffusion in stellar atmospheres is to get as close as possible to the point where numerical models might confidently be confronted with observations. Have we reached that point? Probably not, since atomic diffusion is a very *sensitive* process,[7] and since numerical models could yet be enriched by additional physical processes, especially NLTE effects (Alecian 2015). On the other hand, magnetic field and abundance maps are not directly *observed* but instead result from inversion techniques based on a number of assumptions that are yet in need to be confirmed by independent methods/simulations/codes. Let us just mention the unsolved questions of horizontal pressure equilibrium and of multiple solutions to Zeeman Doppler inversions as discussed by Stift & Leone (2017). We prefer to look at published ZD maps as being part of an *observational model*, giving good fits to the observed Stokes spectra, but based on some strictly mathematical hypothesis for the inversion method, and possibly suffering from inadequate physical constraints concerning the magnetic geometry. Still, an attempt at comparison may be justified in the present case because the

[7]Easily perturbed by other processes (see Section 1).

atmospheric model we have used has parameters ($T_{\rm eff} = 10\,500$ K, $\log g = 3.6$) intentionally quite close to those of θ Aurigae as determined by Kochukhov et al. (2019), whose observational model is provided through maps for the abundances of Cr and Fe together with magnetic maps. The respective field geometries are different (apart from the dominant dipolar field direction), but their maximum field strength ($\approx$1.0 kG) is lower than ours (1.5 kG).

5.2.1 Calcium comparison

Kochukhov et al. (2019) do not provide maps for calcium distribution; however, these authors have determined an average underabundance of Ca (−0.8 dex with respect to the Sun) for θ Aurigae, which is compatible with the underabundances we find (Fig. 4).

5.2.2 Chromium comparison

For chromium, Kochukhov et al. (2019) find a large average overabundance with respect to the Sun (about +2 dex), something we clearly do not find in our numerical model. This could suggest that our mass-loss models do not apply well to this star (too large a mass-loss rate). Strangely, their Cr abundance map looks like our results of Alecian & Stift (2017), which were obtained through equilibrium solutions and for much stronger magnetic fields (despite Kochukhov et al. 2019, claimed that theoretical models are in disagreement with observations). The only aspect that is in common between their observational model and our results shown in Fig. 5, (model B) is the underabundant ring at the magnetic equator.

5.2.3 Iron comparison

According to Kochukhov et al. (2019), iron appears to be overabundant in θ Aurigae by about +1 dex on average. We find overabundances also in layers above $\log \tau_{5000} \approx -1.0$ for the three models of mass-loss (Fig. 7), but Fe appears rather depleted in deeper layers (these layers contribute to refill the upper ones). Concerning the observational model of the Fe distribution of Kochukhov et al. (2019), it clearly is affected – as for Cr – by the magnetic geometry, since Fe appears to be less overabundant (almost solar) on the magnetic equator, but not only there. Indeed, outside the magnetic equator, their Fe distribution seems only loosely correlated with the magnetic geometry: It is sometimes less enhanced at positions where the field strength is very low in both components (radial and horizontal); sometimes the reverse is true. In our magnetic geometry, there is no such weak magnetic structure. Our computations reveal depleted iron essentially at the magnetic equator for mass-loss model B and slabs deeper than $\log \tau_{5000} \approx -1.0$.

5.2.4 How to interpret discrepancies?

Clear differences appear when we attempt a direct comparison of our numerical models with the observational model of θ Aurigae. We will not discuss the validity of the observational model although it could possibly be at the origin of the discrepancies. In the present case, the most significant disparity is found between the average overabundance of Cr determined for θ Aurigae and our calculations, even though Cr is well supported by the radiative acceleration.[8]

[8]In the equilibrium solution, large radiative accelerations necessarily correspond to large overabundances. This is generally not the case in time-dependent solutions.

Noting that average abundances of Kochukhov et al. (2019, their table 1) have been obtained by classical methods (independently from their inversion), we are relatively confident of these average abundances. Our numerical model features mainly one overabundance spot in high layers (model B), all the remaining parts of the atmosphere being underabundant. The simplest way to explain this lack of average Cr overabundance is to incriminate our models of anisotropic mass-loss (Fig. 3), which could involve overly large mass-loss rates. Remember that large mass-loss rate impede the build-up of abundance stratifications. Presently, we are still treating the mass-loss rate as a free parameter (direct measurements are not available) that is adjusted according to numerical constraints imposed by our code CARATMOTION. This is certainly a weakness of our computations that we hope to overcome in the near future. Another explanation comes from the boundary condition that we have to enforce at the deepest layer of the atmospheric model. Because we do not know how elements diffuse below the atmosphere, we keep the abundances constant in time, equal to their solar values. In general, this is justified, since diffusion time-scales in these depths are $\gtrsim 10^5$ yr (several orders of magnitude larger than in upper layers), but it might prove problematic for evolved stars like θ Aurigae.

6 CONCLUSIONS

In this study, we have calculated the time-dependent diffusion of Ca, Cr, and Fe for a magnetic atmosphere with parameters very close to those of θ Aurigae, taking into account stellar mass-loss. We have considered two models of anisotropic mass-loss where the rates decrease from the magnetic pole to the equator, and one model (model C) with a constant mass-loss rate of $2.0\,10^{-14}$ solar mass per year. Computing a grid of 1D models of atmospheres with stratified abundances, we produce a 3D atmosphere with a given non-axisymmetric magnetic geometry. The mass-loss rate is a free parameter in our calculations, but numerical constraints prevent us to be as free in our choice as we would like to be, since numerical convergence is hardly possible for mass-loss rates smaller than the one underlying model C (see Section 5.2.4). Let us recall however at this point that presently our CARATMOTION code constitutes the most advanced software capable of computing fairly self-consistent CP star atmospheres with inhomogeneous distributions of elements resulting from atomic diffusion.

Several kinds of abundance distributions have been obtained, from spot-like overabundances to ring-like structures (both with over- and underabundances), depending on the element and mass-loss model. The warped ring-like structures figure prominently. This is certainly related to the magnetic geometry we have adopted because even though it is non-axisymmetric, the dipolar component dominates. Comparison of element distributions we obtain, with the θ Aurigae observational model of Kochukhov et al. (2019) turns out rather unsatisfactory, even if some compatibility can be found, essentially concerning ring-like underabundances.

ACKNOWLEDGEMENTS

Most of the codes that have been used to compute the grid of models have been compiled with the GNAT GPL Edition of the Ada compiler provided by AdaCore; this valuable contribution to scientific computing is greatly appreciated. This work has been supported by the Programme National de Physique Stellaire (PNPS) of CNRS/INSU, France, and performed using HPC resources from GENCI-CINES (grants c2019045021, c2020045021). 3D reconstructions have been carried out using the software © IGOR PRO (V8). The authors want to

thank Dr. Günther Wuchterl, head of the 'Verein Kuffner-Sternwarte', for the hospitality offered.

DATA AVAILABILITY

The data underlying this paper will be shared on reasonable request to the corresponding author.

REFERENCES

Alecian G., 1996, A&A, 310, 872
Alecian G., 2015, MNRAS, 454, 3143
Alecian G., Stift M. J., 2004, A&A, 416, 703
Alecian G., Stift M. J., 2006, A&A, 454, 571
Alecian G., Stift M. J., 2010, A&A, 516, A53+
Alecian G., Stift M. J., 2017, MNRAS, 468, 1023
Alecian G., Stift M. J., 2019, MNRAS, 482, 4519
Alecian G., Vauclair S., 1981, A&A, 101, 16
Alecian G., Stift M. J., Dorfi E. A., 2011, MNRAS, 418, 986
Asplund M., Grevesse N., Sauval A. J., Scott P., 2009, ARA&A, 47, 481
Babcock H. W., 1947, ApJ, 105, 105
Babel J., 1992, A&A, 258, 449
Bischof K. M., 2005, Mem. Soc. Astron. Ital. Suppl., 8, 64
Borsenberger J., Praderie F., Michaud G., 1981, ApJ, 243, 533
Deutsch A. J., 1956, PASP, 68, 92
Deutsch A. J., 1957, AJ, 62, 139
Kochukhov O., Shultz M., Neiner C., 2019, A&A, 621, A47
Kurucz R. L., 2005, Mem. Soc. Astron. Ital. Suppl., 8, 14
Landstreet J. D., Dolez N., Vauclair S., 1998, A&A, 333, 977
LeBlanc F., Monin D., Hui-Bon-Hoa A., Hauschildt P. H., 2009, A&A, 495, 937
Michaud G., 1970, ApJ, 160, 641
Michaud G., Charland Y., Megessier C., 1981, A&A, 103, 244
Michaud G., Tarasick D., Charland Y., Pelletier C., 1983, ApJ, 269, 239
Michaud G., Alecian G., Richer J., 2015, Atomic Diffusion in Stars, Astronomy and Astrophysics Library, Springer International Publishing, Switzerland
Ndiaye M. L., LeBlanc F., Khalack V., 2018, MNRAS, 477, 3390
Oksala M. E., Silvester J., Kochukhov O., Neiner C., Wade G. A., MiMeS Collaboration, 2018, MNRAS, 473, 3367
Ryabchikova T., 2005, in Alecian G., Richard O., Vauclair S., eds, EAS Publ. Ser. Vol. 17, Proceedings of Element Stratification in Stars: 40 Years of Atomic Diffusion. p. 253
Stibbs D. W. N., 1950, MNRAS, 110, 395
Stift M. J., Leone F., 2017, ApJ, 834, 24
Stift M. J., Hubrig S., Leone F., Mathys G., 2013, in Shibahashi H., Lynas-Gray A. E., eds, ASP Conf. Ser. Vol. 479, Progress in Physics of the Sun and Stars: A New Era in Helio- and Asteroseismology. Astron. Soc. Pac., San Francisco, p. 125
Vauclair S., 1975, A&A, 45, 233
Vauclair S., Hardorp J., Peterson D. M., 1979, ApJ, 227, 526
Vick M., Michaud G., Richer J., Richard O., 2010, A&A, 521, A62

This paper has been typeset from a TEX/LATEX file prepared by the author.